Metastable phase solidification in electron beam welding of dissimilar stainless steels

S. Tsukamoto and H. Harada
National Research Institute for Metals, 2-3-12, Nakameguro, Meguro-ku, Tokyo (Japan)
H. K. D. H. Bhadeshia
University of Cambridge, Department of Materials Science and Metallurgy, Pembroke Street, Cambridge CB2 3QZ (UK)

Abstract

Electron beam welds between dissimilar stainless steels with different solidification modes were studied with a view to elucidating the role of nucleation, cooling rate and direction of dendrite growth on the tendency towards metastable phase solidification. The results are compared with the solidification behaviour of levitation melted samples. It is demonstrated that with careful design, stainless steels which normally solidify as ferrite can be induced into metastable austenitic solidification by removing the barrier to the nucleation of austenite. This is achieved in practice by allowing stable dendrites of austenite to continue growth into the liquid which normally solidifies to ferrite; it is found that the direction of growth of the dendrites has to be carefully controlled.

1. Introduction

The solidification mode of stainless steel weld metal is normally classified into four types such as austenitic (A), austenitic–ferritic (AF), ferritic–austenitic (FA) and ferritic (F). The ratio of Cr equivalent Cr_{eq} to Ni equivalent Ni_{eq} can often be used to predict the fraction of ferrite and austenite at room temperature in conventional stainless steel welds [1–4]. However, rapid solidification using high power density beams can change the solidification mode from ferritic to asutenitic even though the thermodynamically stable phase is ferrite [5–8]. Furthermore, if the need to nucleate metastable austenite can be avoided, then the cooling rate necessary to induce metastable solidification of austenite can be reduced [9]. The aim of the present work was to extend some earlier studies dealing with metastable austenite formation [9], using elecron beam welding as the energy source, and to clarify the role of the nucleation process by comparing the welding experiments with a levitation melting method in which contact with a substrate is avoided.

2. Experimental procedure

Seven commercial stainless steels were used in the present work. The chemical compositions are listed in Table 1, where the letters E and L in materials indicate electron beam welding and levitation melting respectively. The solidification modes given in Table 1 were determined using differential scanning calorimetry (DSC).

2 mm thick stainless steels with different solidification modes of AF (steel A, 310S) and FA (steel B) were combined together and full penetration electron beam weldings were carried out across the junction from steel A to steel B as shown in Fig. 1(a). The heat input, and hence the cooling rate, were varied by choosing a welding speed in the range 4.2–83.3 mm s^{-1}. The beam focal point was located just on the sample surface.

An alternative joint geometry was also examined to promote the formation of metstable austenite. Steel 310S was overlaid with FA mode steels 0.25–0.40 mm thick. Lap weldings were then carried out to allow the growth of austenite dendrites from the bottom of partial penetration electron beam welds (Fig. 1(b)). The electron beam was focused just on the sample surface and deflected circularly (amplitude 0.25 mm, frequency 2 kHz) to maintain a parallel bead width along the penetration. The beam current was reduced gradually during welding so that the electron beam could penetrate just below the dissimilar steel interface at the start of the weld and then only penetrate the top sheet as the weld continued. In this way, the austenite dendrites from the underlying 310S could be induced to continue metastable growth into the undiluted FA mode steels.

0921-5093/94/$7.00
SSDI 0921-5093(93)04535-P

TABLE 1. Chemical compositions of materials

Material	Cr	Ni	Mn	C	Si	P	S	Mo	Cr_{eq}	Ni_{eq}	Cr_{eq}/Ni_{eq}	Solidification mode
304 E	18.23	8.61	0.83	0.06	0.47	0.031	0.005		18.94	10.83	1.75	FA
316 E	16.79	10.74	1.34	0.04	0.67	0.034	0.003	2.05	19.85	12.61	1.57	FA
316 LE	17.31	12.09	1.29	0.01	0.71	0.035	0.002	2.12	20.50	13.07	1.57	FA
310SE	25.05	19.02	0.79	0.04	0.73	0.015	0.001		26.15	20.62	1.27	AF
301L	17.00	7.32	0.93	0.09	0.67	0.032	0.004	0.14	18.15	10.48	1.73	FA
304L	18.25	10.24	1.41	0.03	0.35	0.034	0.003		18.77	11.84	1.60	FA
316L	17.71	11.75	0.83	0.05	0.47	0.025	0.005	2.11	20.53	13.67	1.50	FA

$Cr_{eq} = [Cr] + [Mo] + 1.5[Si] + 0.5[Nb]$; $Ni_{eq} = [Ni] + 30[C] + 0.5[Mn]$.

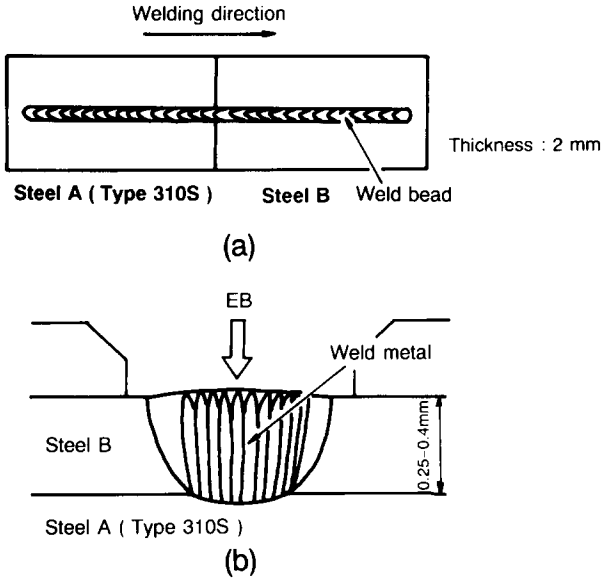

Fig. 1. Electron beam welding of dissimilar stainless seels: (a) butt welding, (b) lap welding.

The correlation between undercooling ΔT and the phase selection in undercooled liquid was also examined using a levitation melter which can avoid heterogeneous nucleation from container walls. Three commercial FA mode stainless steels (Table 1) were levitated in a vacuum chamber which was back filled with Ar–10%H_2 gas. The 700 mg samples were melted and solidified in the levitation coil by controlling the flow rate of He–10%H_2 cooling gas under the constant power of the induction coil. When a recalescence event wsa recognized, the power was shut down and the sample quenched in a tin bath. The temperature of the samples was measured using a pyrometer.

3. Electron beam welding of dissimilar stainless steels

When 316L was butt welded to 310S, metastable austenite dendrites were found in 316L welds for the lowest welding speed of 4.2 mm s^{-2}, whereas all the 316L weld metal showed FA mode solidification in autogenous welding. A horizontal section is shown in Fig. 2(a) where the austenie dendrites initiated in 310S welds penetrate into 316L welds to a distance of 12.4 mm beyond the junction. Microanalysis confirmed that this was not caused by a dilution effect. However, the formation of metastable austenite was limited to the centre of the welds and it was not found for higher welding speeds or for the other steel welds. This is attributed to the inappropriate growth direction of dendrites caused by the welding geometry. In dissimilar butt welding, as shown in Fig. 2(b), only the dendrites which grow in the welding direction can effectively penetrate the dissimilar metal junction and hence lead to metastable austenitic solidification, but the dendrites are apt to collide with each other at the centre of the welds for a higher welding speed with its associated high cooling rate, since the molten pool geometry varies from elliptical to tear-drop with increasing welding speed.

The joint geometry was therefore redesigned. Lap weldings of dissimilar stainless steels were carried out as shown in Fig. 1(b), so that the austenite dendrites growing from the 310S fusion boundary could continue their growth into FA mode steel welds. Figure 3(a) shows that the method successfully allowed 316 stainless steel to solidify to metastable austenite over a wide region at a welding speed of 33.3 mm s^{-1}. Autogenous welding of 316, however, led to primary ferritic solidification for the same conditions (Fig. 3(b)). Microanalysis again confirmed that this was not a dilution effect. Figure 3(c) shows a summary of the lap welds using 316L and 316. The volume fraction of metastable austenite increases with the welding speed, which might be expected since a larger cooling rate favours the formation of metastable austenite. An additional reason is associated with the growth direction of dendrites. The solidification wall behind the beam cavity has a tendency to be more inclined in a horizontal direction as the welding speed is increased

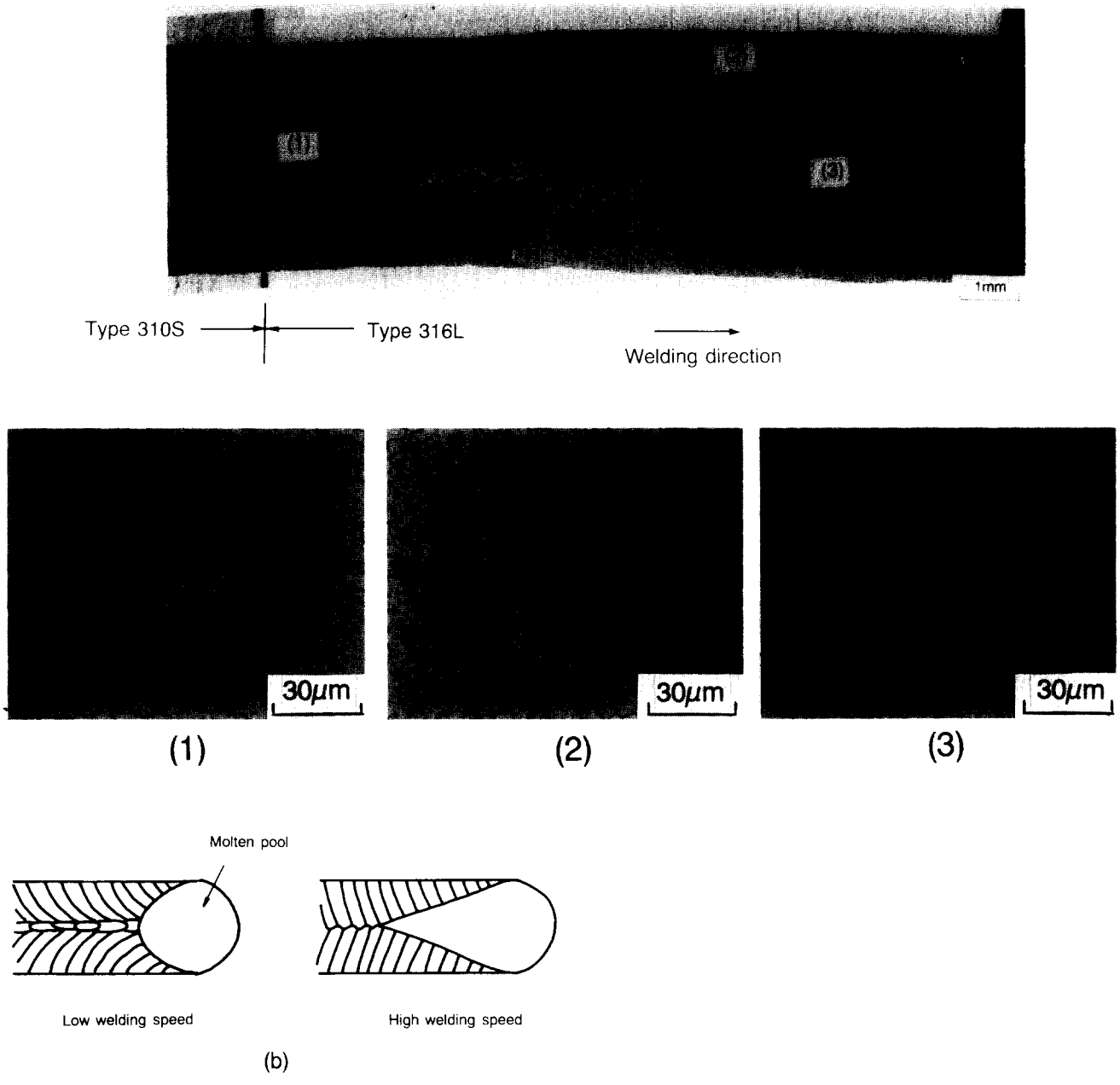

Fig. 2. (a) Horizontal section of butt welds between 310S and 316L (welding speed 4.2 mm s^{-1}); (b) effect of welding speed on the growth direction of dendrites.

[10]. Thus the austenite dendrites initiated at the 310S fusion boundary can penetrate further into the weld metal for higher welding speeds.

These results indicate that metastable austenitic solidification can be induced at relatively low cooling rates, if the nucleation of austenite is rendered unnecessary by the continued growth of austenite across an AF/FA junction, as long as the dendrite growth direction can be controlled.

4. Solidification mode of undercooled liquid (levitation experiments)

As described above, the substrate exerts a great influence on phase selection during liquid–solid transformation. The containerless solidification behaviour of FA mode stainless steel droplets was examined as a function of undercooling, which was controlled by altering the cooling rate in the range 1–65 K s^{-1}. A

levitation melting method was used. The undercooling varied from about 10 to maximum values of 218, 193 and 210 K for 316, 304 and 301 steels respectively. The corresponding microstructures of 316 are shown in Fig. 4. When ΔT is less than 140 K, the microstructure consists of a primary solidified phase (region P) and an intergranular rapidly solidified region (region L) which was liquid prior to quenching as shown in Fig. 4(a). The fraction of the liquid phase decreases with increasing ΔT. X-ray diffraction suggested that these samples contain austenite and a small amount of ferrite. Lamellar structures can be seen in the primary solidified grains over large regions near the centre of the samples. Transmission electron microscopy (TEM) revealed that the lamellar structures consist of austenite and thin layers of ferrite as shown in Fig. 4(b). When the sample was cooled gradually in the levitation coil after solidification at $\Delta T = 54$ K, the second peak was found at 1663 K after a recalescence event. The microstructure which was quenched after the second peak shows vermicular ferrite in a matrix of austenite as shown in Fig. 4(c). If a sample solidifies to primary austenite, then the resultant microstructure should either be fully austenitic or contain some intercellular ferrite. However, the ferrite was observed experimentally to be located inside the cells as shown in Figs. 4(b) and 4(c). Thus, the primary solidification may have been to ferrite for these particular samples, most of the ferrite subsequently transforming to austenite in spite of the fact that the samples were rapidly cooled using a molten tin bath. For these reasons, it is difficult to use metallography alone to determine the first solid phase that forms.

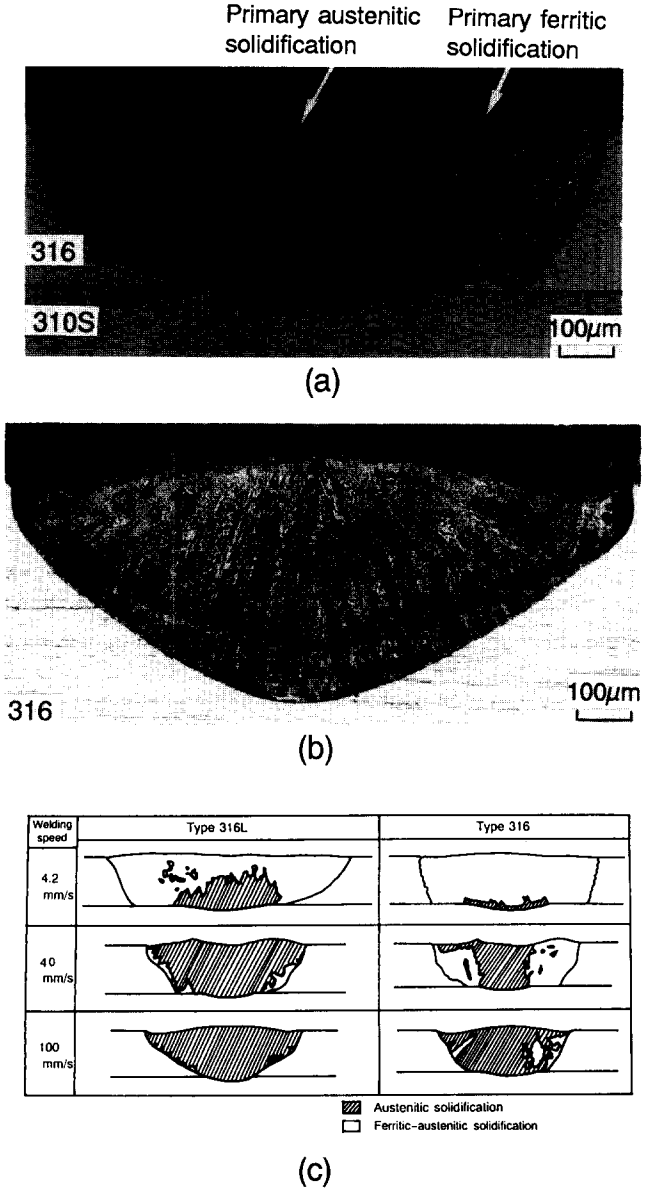

Fig. 3. (a) Horizontal section of lap welds between 316 and 310S (welding speed 33.3 mm s^{-1}); (b) horizontal section in autogenous welds of 316 (welding speed 33.3 mm s^{-1}); (c) effect of welding speed on the formation of metastable austenite in lap welding.

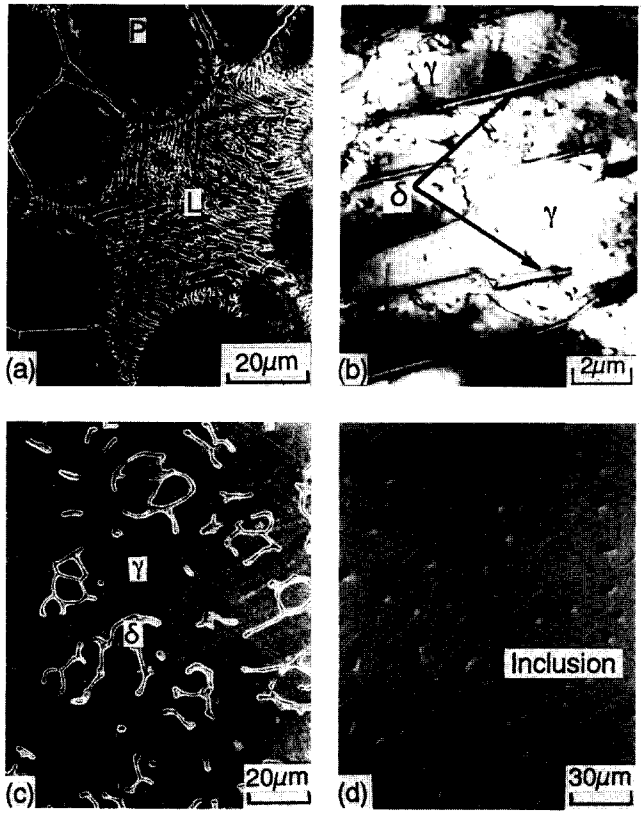

Fig. 4. Microstructures of levitation melted 316 steels: (a) $\Delta T = 12$ K (L, liquid; P, primary crystal); (b) TEM image of lamellar structure, $\Delta T = 96$ K; (c) $\Delta T = 54$ K; (d) $\Delta T = 180$ K. Samples (a), (b) and (d) were quenched soon after a recalescence event. Sample (c) was quenched after recognizing a second peak of the temperature.

The chemical segregation behaviour was therefore examined in order to throw more light on the identification of the primary solidification phase in these samples. Figure 5 shows the distributions of Ni and Cr in the specimen illustrated in Fig. 4(a) where Ni is highly enriched and Cr is a little depleted in the liquid phase. Similar distributions can be seen in all the samples whenever the undercooling was less than 140 K. The partitioning coefficients of some of the elements were calculated for both cases of primary ferritic and austenitic solidification, using the MTDATA package [11] to identify the primary phase. The results are shown in Table 2. The partitioning coefficient of Ni is much smaller and that of Cr is a little larger than unity when the samples solidify to ferrite. This tendency is in good agreement with the observed segregation behaviour and means that the primary solidification phase is ferrite when the undercooling is less than 140 K.

When the undercooling exceeded 180 K, microstructures which were completely different from those associated with smaller undercoolings were observed. Submicrometre inclusions could be found in the central regions of fully austenitic grains or subgrains, as shown in Fig. 4(d). EPMA analysis revealed the inclusions to be rich in Mo, Cr, P and S. A narrow Cr-depleted and Ni-enriched region surrounded each inclusion. No significant segregation could be observed in the remainder of the microstructure. The samples sometimes revealed signs of shrinkage porosity. Some of the pores traversed grain boundaries and were found to be associated with inclusions. For samples which were rapidly solidified in tin, similar inclusions could be found at the austenite cell boundaries. Furthermore, the partitioning coefficient of Mo which is involved in the inclusion is much smaller in primary austenitic solidification as shown in Table 2. These results lead us to conclude tentatively that the primary phase to solidify at undercoolings larger than 180 K is austenite, where the inclusions are formed at the last stage of solidification and the grain boundaries move after that. A positive alternative interpretation is that at sufficiently large undercoolings, Cr-rich inclusions (which may be sigma phase) precipitate directly from the liquid. The surrounding liquid therefore becomes enriched in austenite stabilizing elements, leading to austenite nucleation and rapid growth. Whatever the detailed interpretation, it is evident that at sufficiently large undercoolings, the primary solidification phase is austenite, because these samples show fully austenitic microstructures. Further experimental work is necessary to clarify these issues, perhaps using a fast response temperature recorder during the recalescence events [12, 13].

The above results indicate that primary ferritic solidification is favoured when the undercooling is less than about 140 K. Unfortunately, the undercooling in electron beam welding is not known, but it should be less than 140 K since the growth of existing phases in the substrate removes the need for nucleation. Thus, the surrounding matrix exerts a great influence on the phase selection. The electron beam lap welding of dissimilar metals is effective in inducing metastable phase solidification in the surface material.

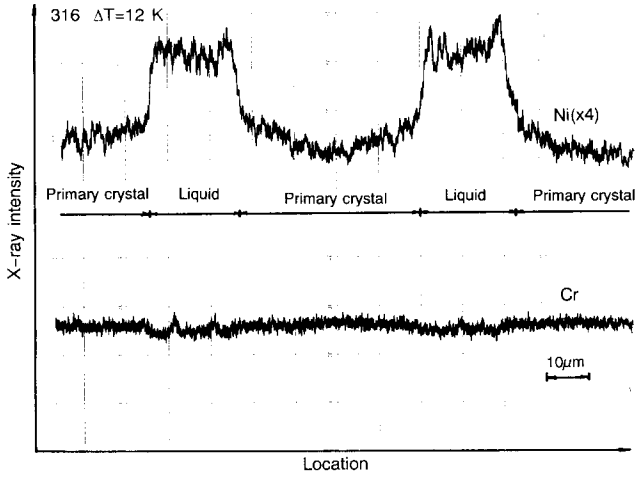

Fig. 5. Distributions of Ni and Cr in the sample as shown in Fig. 4(a).

5. Conclusions

It has been demonstrated that during the electron beam welding of dissimilar stainless steels, thermodynamically stable austenite dendrites initiated in a primary austenitic solidification steel can be induced to continue growth across the weld junction into another stainless steel where ferrite should be the thermodynamically stable phase. The effect can be enhanced by choosing joint geometries and welding conditions which favour dendrite growth across the dissimilar steel junction. Microanalysis of levitation melted FA mode steels has shown that ferrite is favoured as a

TABLE 2. Partitioning coefficients of some elements in primary ferritic and austenitic solidification (316 steel)

Solidification mode	Partitioning coefficient		
	Cr	Ni	Mo
Primary ferritic	1.02	0.78	0.98
Primary austenitic	0.86	1.08	0.69

primary phase over a wide range of undercoolings. The results therefore suggest that the substrate phase around the melt exerts a great influence on the phase selection during the rapid solidification associated with electron beam welding.

Acknowledgments

This work was done under the auspices of the Atomic Arrangement: Design and Control Project, a collaboration between the University of Cambridge and Research Development Corporation of Japan. The authors thank Professor C. J. Hamphreys, Professor M. Yamazaki, and Professor H. Nakae for their useful advice. The authors are also grateful to Dr. R. Thomson, Dr. O. Umezawa and Mr. H. Kobayashi for their help with thermodynamic calculations, micro-analysis and levitation melting respectively.

References

1 A. L. Shaeffler, *Met. Prog., 56* (1949) 680.
2 W. T. DeLong, *Welding J., 53* (1974) 273s.
3 N. Suutala, *Acta Univ. Ouluensis, 26* (1983) 53.
4 N. Suutala, *Metall. Trans. A,14* (1982) 191.
5 J. M. Vitek, A. D. Gupta and S. A. David, *Metall. Trans. A, 14* (1983) 1833.
6 S. Katayama and A. Matsunawa, *Proc. Int. Conf. on Applications of Lasers and Electro-optics '84*, Vol. 44 L.1.A., 1984, p. 60.
7 Y. Nakao, K. Nishimoto and W. P. Zhang, *Proc. 4th Int. Colloq. on Welding and Melting by Electron and Laser Beams*, Vol. 2, 1988, p.673.
8 S. A. David, J. M. Vitek and L. T. Hebble, *Welding J., 66* (1987) 289s.
9 H. K. D. H. Bhadeshia, S. A. David and J. M. Vitek, *Mater. Sci. Technol., 7* (1991) 50. .
10 S. Tsukamoto and H. Irie, *Welding in the World, 23* (1985) 130.
11 MTDATA-Metallurgical and Thermochemical Databank, National Physical Laboratory, Teddington, 1992.
12 M. Barth, K. Eckler and M. Herlach, *Mater. Sci. Eng., A133* (1991) 790.
13 D. M. Herlach, B. Feuerbacher and E. Schleip, *Mater. Sci. Eng., A133* (1991) 795.